IEEE Access
Multidisciplinary | Rapid Review | Open Access Journal

Received October 21, 2019, accepted November 6, 2019, date of publication November 14, 2019,
date of current version November 25, 2019.

Digital Object Identifier 10.1109/ACCESS.2019.2953463

Underwater Image Enhancement Using Scene Depth-Based Adaptive Background Light Estimation and Dark Channel Prior Algorithms

SHUDI YANG, ZHEHAN CHEN, ZHIPENG FENG, (Member, IEEE), AND XIAOMING MA
Department of Mechanical Engineering, University of Science and Technology Beijing, Beijing 100083, China

Corresponding author: Zhehan Chen (chenzh_ustb@163.com)

This work was supported by the National Key Research and Development Program of China, under Grant 2018YFC0810500.

ABSTRACT Due to the complexity of the underwater environment, underwater images captured by optical cameras usually suffer from haze and color distortion. Based on the similarity between the underwater imaging model and the atmosphere model, the dehazing algorithm is widely adopted for underwater image enhancement. As a key factor of the dehazing model, background light directly affects the quality of image enhancement. This paper proposes a novel background light estimation method which can enhance the underwater image. And it can be applied in 30-60m depth with artificial light. The method combines deep learning to obtain red channel information of the background light in the dark channel of the underwater image. Then, the background light is obtained by adaptive color deviation correction. Finally, the experiments of underwater images enhancement are carried out, using the dark channel prior algorithm based on the proposed background light estimation method. The results show that the proposed method effectively improves underwater image blur and color deviation, and is superior to other methods in multiple non-reference image evaluation indicators.

INDEX TERMS Adaptive background light estimation, color correction, deep learning, dark channel prior, underwater image enhancement.

I. INTRODUCTION

With the rapid development of underwater robots, the tasks of underwater environment detection and deep-sea exploration are increasing [1]. Clear underwater images are important for exploring the marine environment and rescuing in underwater. However, the underwater image acquired by the camera has poor visibility, which mostly due to haze caused by light that is reflected from surface and is scattered by water particles, and color deviation caused by the various attenuation degrees of the light varies among different wavelengths [2]–[4]. Also, in a complex underwater environment, both of the fluidity of the water and the constant movement of the object can cause the image becoming blurred.

To date, researchers have made important contributions to underwater image enhancement. He *et al.* [4] proposed a simple and effective dark channel prior model in 2011, which has achieved remarkable results in image dehazing. Then, based on the similarity between the underwater imaging model and atmosphere imaging model, the dark channel prior model has gradually been applied to underwater image restoration. Yang *et al.* [5] implemented a low-complexity underwater image enhancement method based on dark channel prior. Galdran *et al.* [6] proposed a red channel prior model for underwater environments based on dark channel prior and corrected the transmission map in combination with the saturation of the image to achieve natural color correction and visibility improvement. Ding *et al.* [7] estimated the transmission map by scene depth and used the dark channel prior to achieve underwater image dehazing. Finally, the white balance algorithm was used to correct color deviation. Zhu *et al.* [8] integrated the histogram equalization with the dark channel prior, which effectively improved the contrast of underwater images. Ancuti *et al.* [9] improved the accuracy of background light estimation by building on the blending of two images that are directly derived from a color-compensated and white-balanced version of the original degraded image. Xie *et al.* [10] improved the dark channel prior model by estimating the theoretical values of global background light, and used the relationship between the scattering coefficient and the wavelength to calculate the transmission map of the three channels, which better

The associate editor coordinating the review of this manuscript and approving it for publication was Emre Celebi.

solved the problems such as color deviation and blurring caused by background scattering under illumination conditions. Li *et al.* [11] proposed an improved bright channel model, and a corresponding denoising algorithm and color correction method. Akkaynak and Treibitz [12] calculates backscatter using the darkest pixels in the image and their known range information. Then, it uses an estimate of the spatially varying illuminant to obtain the range-dependent attenuation coefficient.

However, existing researches usually focused on improving the dark channel prior algorithm by refining the transmission map and estimating the background light by changing the color channel, whereas ignoring the background light information of the original image provided by the dark channel itself. In this paper, a novel background light estimation method which combined maximum scene depth estimation and adaptive color correction is proposed. The method can improve the brightness of the underwater image, remove the haze and correct the color deviation, only need to correct the background light of the underwater image, and just need a single image as an input.

The remainder of this paper is organized as follows, Section 2 introduces the relevant theories and algorithms used in this paper. Section 3 details the principles of adaptive background light estimation. Experiments were carried out in Section 4 to verify the proposed methods. Finally, we summarize this paper in Section 5.

II. RELATED WORK

A. UNDERWATER IMAGING MODEL

In 1980, McGlamery proposed a classical model of the underwater imaging system in [13], which pointed out that water and a large number of suspended particles can absorb and scatter light, and make underwater images to be color distortion, blurred detail, low overall brightness, and low contrast. According to the underwater optical imaging model shown in Fig.1. The total light intensity I_T received by the underwater imaging system is composed of three partials linear superposition: 1) the direct components I_D reflected by the object; 2) the forward-scattering component I_F which represents the small angle scattering during the object reflection process; 3) the back-scattering component I_B which represents the influence of light scattering caused by the suspended particles.

$$I_T(x,\lambda) = I_D(x,\lambda) + I_F(x,\lambda) + I_B(x,\lambda) \tag{1}$$

where x represents the pixel point in the image and $\lambda \in \{R, G, B\}$ is the color channel.

The energy components I_D, I_F and I_B are exponentially attenuated as they propagate from the target to the imaging device, so the three light components can be represented as:

$$I_D(x,\lambda) = I_0(x,\lambda)\, e^{-c(\lambda)d(x)} \tag{2}$$

$$I_F(x,\lambda) = [I_0(x,\lambda)\, e^{-c(\lambda)d(x)}] * g(x,\lambda) \tag{3}$$

$$I_B(x,\lambda) = A(\lambda)\,[1 - e^{-c(\lambda)d(x)}] \tag{4}$$

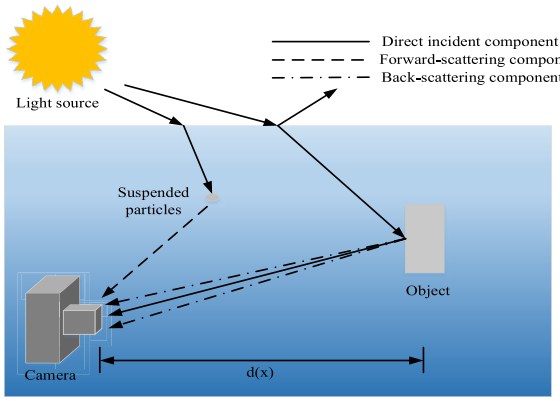

FIGURE 1. Underwater imaging model [10].

where $I_0(x,\lambda)$ is the light intensity at the location of the object, $c(\lambda)$ is the total attenuation coefficient caused by the absorption and scattering of the light, $d(x)$ is the distance between the object and the camera, and can also be seen as scene depth, $e^{-c(\lambda)d(x)}$ is the underwater transmission map expressed by $t_0(x,\lambda)$, $*$ is the convolution operation, $g(x,\lambda)$ is the point spread function, and $A(\lambda)$ is the background light of λ channel. Comprehensive (1)-(4), the total light intensity received by the camera can be expressed as:

$$I_T(x,\lambda) = [I_0(x,\lambda) + I_0(x,\lambda) * g(x,\lambda)]\, e^{-c(\lambda)d(x)} + A(\lambda)\,[1 - e^{-c(\lambda)d(x)}] \tag{5}$$

The target reflection image $J(x,\lambda)$ is defined as:

$$J(x,\lambda) = I_0(x,\lambda) + I_0(x,\lambda) * g(x,\lambda) \tag{6}$$

Then equation (5) can be reduced to:

$$I_T(x,\lambda) = J(x,\lambda)\, t_0(x,\lambda) + A(\lambda)\,[1 - t_0(x,\lambda)] \tag{7}$$

where, $I_T(x,\lambda)$ is equivalent to low-quality underwater image, and J(x, λ) is clear image. In summary, accurate prediction of underwater transmission map $t_0(x,\lambda)$ and background light $A(\lambda)$ is essential for underwater image enhancement.

Also, as shown in Fig. 2. When light propagates underwater, the underwater attenuation of light vary among different

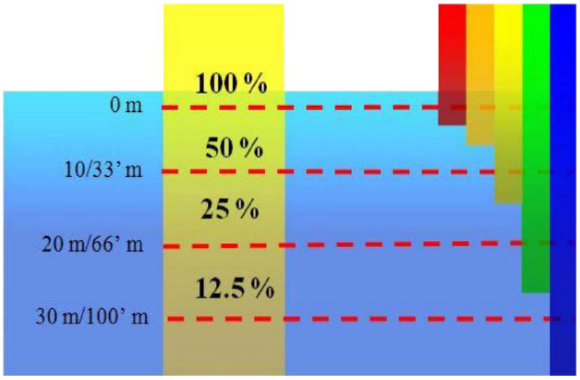

FIGURE 2. Underwat attenuation of light with different wavelengths [13].

wavelengths, in which red light has longer wavelengths and lower frequencies. Therefore, red light is attenuated faster than blue and green light, which makes the underwater image blue-green tone [14], [15].

B. DARK CHANNEL PRIOR

He *et al.* [4] proposed that most local patches in haze-free outdoor images contain some pixels which have very low intensities in at least one color channel [4], which is:

$$J_{dark}(x) = \min_{c\epsilon\{r,g,b\}} \left(\min_{y\epsilon\Omega(x)} \left(J^c(y) \right) \right) \to 0 \tag{8}$$

where J is a haze $-$ free outdoor image, J^c and $J_{dark}(x)$ is a color channel and a dark channel of J, and $\Omega(x)$ is a local patch centered at x. The dark channel prior states that except for the sky region, the intensity of $J_{dark}(x)$ is low and tends to be zero. According to the dark channel prior and the traditional air-based mathematic image acquirement model, the transmission map is calculated by

$$\min_{c\epsilon\{r,g,b\}} \left(\min_{y\epsilon\Omega(x)} \left(I^c(y) \right) \right) = \min_{c\epsilon\{r,g,b\}} \left(\min_{y\epsilon\Omega(x)} \left(J^c(y)\, t(x) + A^c \left[1 - t(x) \right] \right) \right) \tag{9}$$

$$t(x) = 1 - \omega \min_{c\epsilon\{r,g,b\}} \min_{y\epsilon\Omega(x)} \left(\frac{I^c(y)}{A^c} \right) \tag{10}$$

where the value of ω is between 0 and 1 according to application-based. Atmospheric light A^c is calculated by initially choosing the 0.1% brightest pixels of the image. Finally, the dehazing image can be obtained.

$$J^c(x) = \frac{I^c(x) - A(\lambda)}{\max(t(x), t_0)} + A(\lambda) \tag{11}$$

where t_0 is a constant, in order to avoid the $t(x)$ is close to zero and the value of $J^c(x)$ is infinite. The value of t_0 should be set according to the actual situation.

C. FULLY CONVOLUTIONAL RESIDUAL NETWORKS

Laina *et al.* [16] proposed a new method to solve the depth estimation problem of a single image. The method replaced the fully-connected layer, which was part of the original architecture, with the novel up-sampling blocks and used the reverse Huber [17], [18] as loss function to improve the convolutional neural network. Compared to a typical convolutional neural network (CNN), the model is not only simpler than existing methods, can be trained with less data in less time, but also achieves higher quality results. The proposed architecture builds upon Res Net-50[19], and the network is trained using NYU Depth v2 [20] and Make3D [21] datasets respectively.

Ultimately, the method achieves more accurate depth estimation of a single image. The method code is open-source and can be downloaded at https://github.com/iro-cp/FCRN-DepthPrediction.

III. ADAPTIVE BACKGROUND LIGHT ESTIMATION

Equation (11) indicates that the acquisition of background light $A(\lambda)$ has a crucial influence on the clear image $J(x, \lambda)$. Fig.3 shows the underwater image enhancing process. The background light estimation in this paper can be divided into the following steps:

1) The scene depth is accurately estimated by pre-processing the underwater blurred image with CLAHE which can enhance the contrast of blurred images;

2) Using the Fully Convolutional Residual Networks (FCRN) to estimate the depth of the underwater image and find the maximum scene depth $d_{max}(x, \lambda)$;

3) Obtaining the RGB values (A_r, A_g, A_b) at the maximum scene depth in the dark channel map;

4) Using the RGB values of the maximum scene depth in the original image to obtain the ratio of the three color lights, represented by $\alpha_{r,g}, \alpha_{r,b}$;

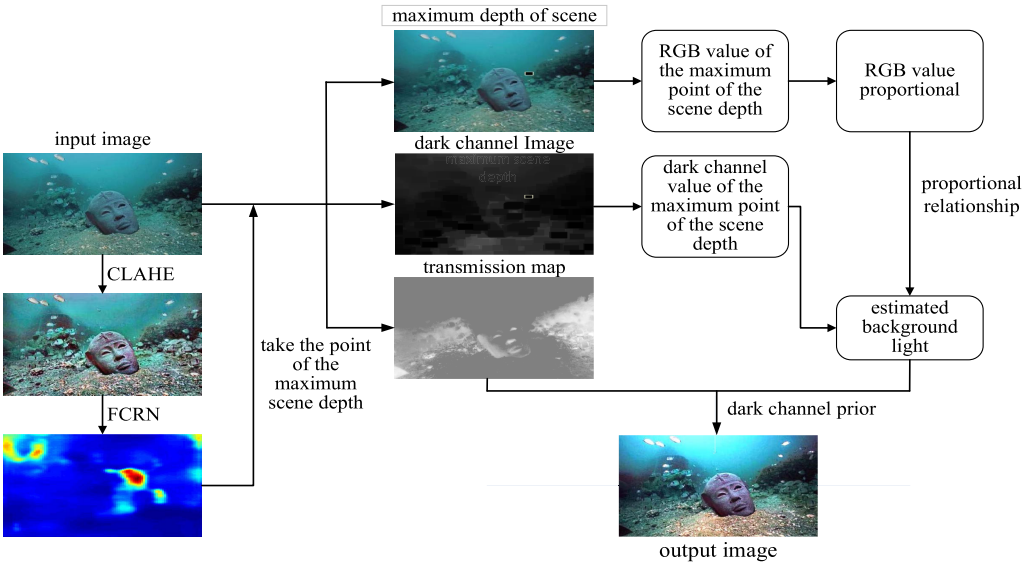

FIGURE 3. Underwater image enhancing process.

5) Based on A_r, adjust the green channel and blue channel values proportionally to get A'_g, A'_b, and as the final background light $A(\lambda) = (A_r, A'_g, A'_b)$;

6) Finally, the dark channel prior and the new background light are used to enhance the underwater image.

A. UNDERWATER IMAGE PREPROCESSING

Underwater images usually has the characteristics of blur, color deviation and low contrast. To obtain a more accurate scene depth, underwater images need to be pre-processed. Zhu *et al.* [22] experimented with a large number of haze images and found that the haze is positively correlated with the difference between the brightness and saturation of the image in the HSV color space. Based on the relationship between scene depth and haze, the relationship between scene depth, brightness and saturation can be derived as below:

$$d(x) \propto c(x) \propto v(x) - s(x) \tag{12}$$

where $d(x)$ is the scene depth at point x in the image, $c(x)$ is the concentration of the haze, the brightness of the scene is represented by $v(x)$, and s(x) is the saturation. Also, contrast is an important measure of image brightness and saturation. Therefore, we should select the method that can effectively improve the image brightness, saturation and contrast to preprocess the underwater image, thus reducing the influence of haze on the scene depth estimation. In this paper, we use contrast limited adaptive histogram equalization (CLAHE) [23], dark channel prior [4], gray world algorithm [24], Automatic Color Enhancement (ACE) [25], Lab Color Correction (LAB)[26], Non-Local Dehazing (NLD) [27] and Screened Poisson equation (SP) [28] to preprocess underwater images separately.

Fig. 4 shows that the enhanced images obtained by preprocessing with the various methods and the corresponding scene depth map. And the enhanced image processed by the CLAHE, ACE, and SP methods works well. Although the enhancement of the ACE method is the best, the method reduces some of the valid information in the original image, so that the resulting depth information is not complete. The CLAHE method enhances noise, but it retains richer depth information. The ultimate goal of this step is to obtain more accurate scene depth information. Therefore, CLAHE is finally selected to preprocess the underwater image. The depth prediction method used in Fig. 4 is detailed in Section B.

B. UNDERWATER IMAGE SCENE DEPTH PREDICTION

Image depth estimation can be obtained by analyzing image features and depth cameras [29]. For example, the distance between the object and the camera can be predicted by

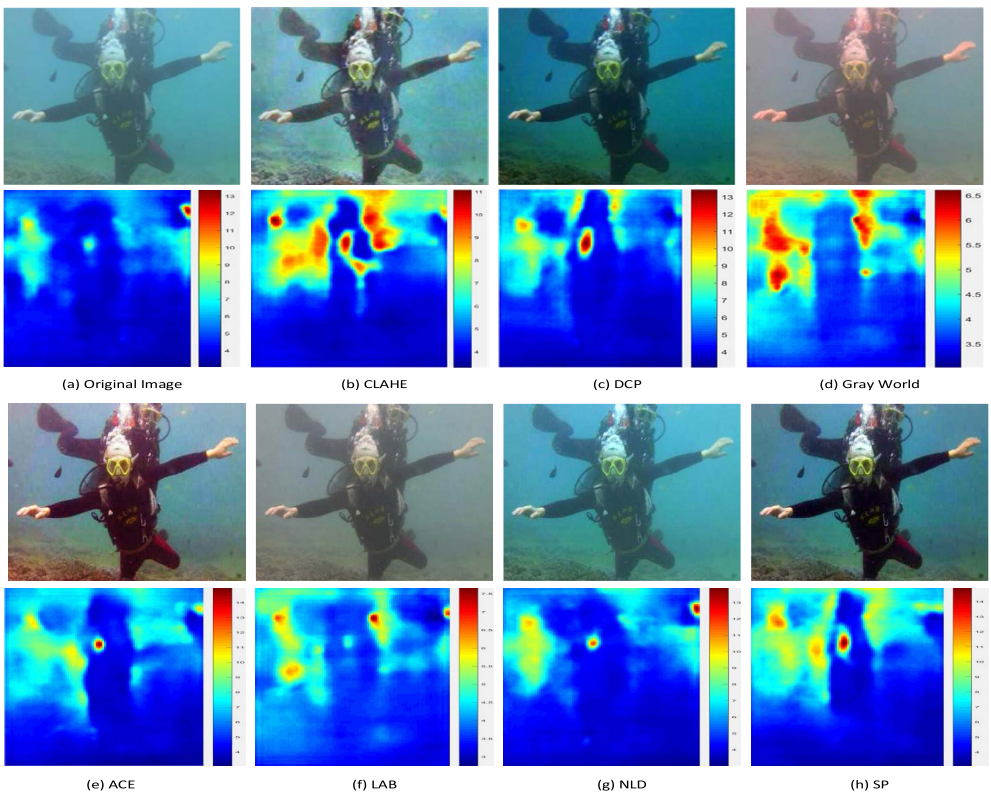

FIGURE 4. Underwater image depth prediction. (a) Original image(up) and scene depth map(down). (b) Pretreated by CLAHE(up) and scene depth map(down). (c) Pretreated by dark channel prior(up) and scene depth map(down). (d) Pretreated by gray world(up) and scene depth map(down). (e) Pretreated by ACE (up) and scene depth map(down). (f) Pretreated by LAB(up) and scene depth map(down). (g) Pretreated by NLD(up) and scene depth map(down). (h) Pretreated by SP(up) and scene depth map(down).

evaluating the haze in the image based on the relationship between the haze and the scene depth. The dark channel priori theory indicates that, when the atmosphere is homogenous, the transmission map $t(x, \lambda)$ can be expressed as:

$$t(x, \lambda) = e^{-\beta d(x,\lambda)} \tag{13}$$

where β is the scattering coefficient of the atmosphere. Equation (13) indicates that the transmission map $t(x, \lambda)$ is attenuated exponentially with the scene depth $d(x)$. Then, the scene depth d(x, λ) can be expressed by:

$$d(x, \lambda) = \frac{-\log t(x, \lambda)}{\beta} \tag{14}$$

Equation (14) indicates that, in theory, we can obtain the scene depth through the transmission map $t(x, \lambda)$ and the atmospheric scattering coefficient β. However, the formula (13) is established with the condition that the atmosphere is homogenous. For the underwater environment, not only the particulate matter but also the density of water is not uniform. The scattering coefficient β changes with the water environment and the specific value cannot be obtained. Fig.5 shows the scene depth map of the same image with the different values of β and it reflects that the value of β has a great influence on the scene depth estimation. In the case of β unknown, accurate scene depth cannot be obtained.

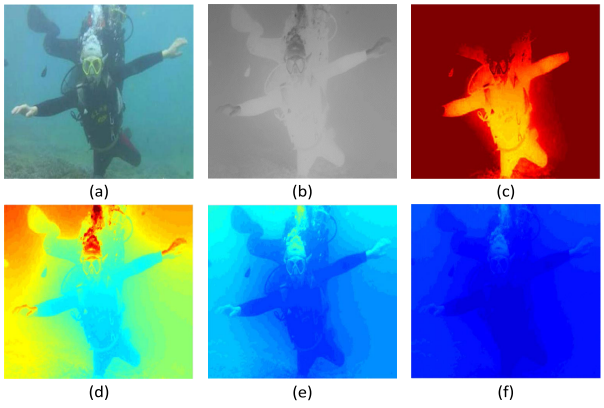

FIGURE 5. Scene depth map of the same image with different β (a) Original underwater image. (b) Transmission map. (c) $\beta = 0.5$, Scene depth map. (d) $\beta = 1$, Scene depth map. (e) $\beta = 2$, Scene depth map. (f)$\beta = 4$, Scene depth map.

It is difficult to obtain accurate scene depth using depth camera and feature analysis, which is caused by the inconvenience of depth camera operation and the difference of β in different waters. It is effective to restore the visual quality of the images with statistical priors [30]. Deep learning has the advantage of efficient and accurate feature extraction based on statistical prior. Therefore, this paper selects the full convolutional residual networks (FCRN) [16] trained by Make3D dataset and NYU Depth v2 dataset to estimate the depth of the underwater image. The error of networks in estimating the scene depth can be as low as 0.127, which fully meets our requirements for accuracy of scene depth. Fig.6 shows the effect of the network on the depth estimation

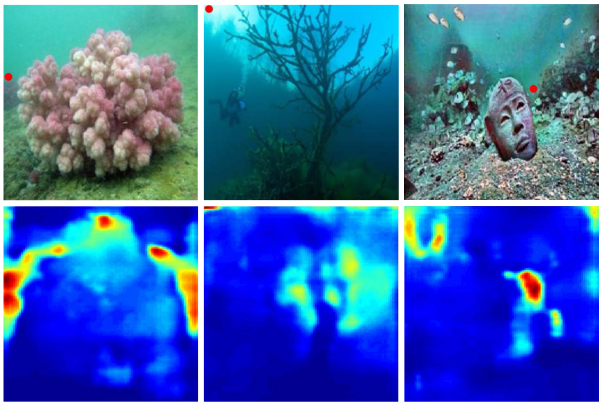

FIGURE 6. Scene depth map of the underwater image.

of underwater pictures. It can be easily seen that the reddish part of the color is the distant view area, the blue part is the near view area, and the darkness of the color represents the distance. The red circle point in Fig.6 represents the maximum scene depth.

C. ADAPTIVE BACKGROUND LIGHT ESTIMATE

According to equations (7) and (13), based on the inverse relationship between the scene depth and the transmission map, it can be concluded that the transmission map is approximately zero at the infinity of the scene depth, and the image $I_T(x, \lambda)$ is equal to the background light $A(\lambda)$. So we can assume that the background light of the image is at the maximum scene depth.

Derivation of equation (11) as follows:

$$\begin{aligned} J(x, \lambda) &= \frac{I_T(x, \lambda) - A(\lambda)}{t_0(x, \lambda)} + A(\lambda) \\ &= \frac{I_T(x, \lambda)}{t_0(x, \lambda)} - \frac{A(\lambda)}{t_0(x, \lambda)} + A(\lambda) \\ &= \frac{I_T(x, \lambda)}{t_0(x, \lambda)} - A(\lambda)\left[\frac{1}{t_0(x, \lambda)} + 1\right] \end{aligned} \tag{15}$$

The larger the gray level, the brighter the image [31]. For equation (15), in the case where $I_T(x, \lambda)$, $t_0(x, \lambda)$ are known and fixed, the smaller $A(\lambda)$, the larger $J(x, \lambda)$. The dark channel is obtained from the three-channel minimum, that is, the gray level of the dark channel is smaller than the corresponding original image. Underwater images are usually dark due to lighting problems. In the case of enhancing the underwater image, the image which taking the point in the dark channel as the background light is brighter than the image obtained by taking the point in the original image as the background light. Therefore, in this paper, the background light is corrected based on the point of maximum depth of the dark channel and the three channel values of the point are recorded as (A_r, A_g, A_b).

Besides, we also need to define the position of the maximum scene depth (the red circle point in Fig.6.) and record it as $M(x_{i,j}, \lambda)$, where $x_{i,j}$ is expressed as the maximum scene depth, i, j are the position coordinates of the point x,

and λ represents the color channel. It should be noted that the resolution of the image after the FCRN will be changed. Assuming that the resolution of the original image is $m \times n$, and the resolution of the depth map is $p \times q$. The positional coordinates corresponding to the maximum scene depth of the original image are calculated by the following equation:

$$M\left(x_{i,j},\lambda\right) = \min_{i\epsilon p}(\min_{j\epsilon q} Depth(x_{i,j})), \quad \lambda \in \{R, G, B\} \tag{16}$$

$$i' = \frac{m \times i}{p}, \quad i' \in \{Z\} \tag{17}$$

$$j' = \frac{n \times j}{q}, \quad j' \in \{Z\} \tag{18}$$

where i', j' are respectively represented as coordinates at the maximum scene depth of the original image, i' and j' and rounded to integer, and $Depth(x_{i,j})$ represents the scene depth map obtained by FCRN. The ratio of the maximum scene depth (i.e., background light) of the original underwater image is as follows:

$$\alpha_{r,g} = \frac{M'\left(x_{i',j'}, g\right)}{M'\left(x_{i',j'}, r\right)} \tag{19}$$

$$\alpha_{r,b} = \frac{M'\left(x_{i',j'}, b\right)}{M'\left(x_{i',j'}, r\right)} \tag{20}$$

where $\alpha_{r,g}$, $\alpha_{r,b}$ represent the ratio of the green channel and the blue channel to the red channel at the point $M'(x_{i',j'}, \lambda)$. We can easily know the degree of color deviation through the above ratio, and then the background light can be corrected.

$$A'_g = \alpha_{r,g} \times A_g \tag{21}$$

$$A'_b = \alpha_{r,b} \times A_b \tag{22}$$

In the above equations, A'_g and A'_b are the values of the corrected G channel and B channel, so the final background light can be expressed as $A(\lambda) = (A_r, A'_g, A'_b)$. Next, the underwater image is processed by dark channel prior based on the adaptive background light correction.

IV. EXPERIMENTAL VALIDATION

We performed image enhancement experiments on a large number of underwater images and evaluated the effectiveness of the method in this paper through subjective visual, questionnaire and objective data. Unfortunately, many authors do not release the implementation of their algorithms. An implementation that relies only on what authors described in their papers does not guarantee the accuracy of the enhancement process and can mislead the evaluation of an algorithm. Consequently, we selected those algorithms for which we could find a trustworthy implementation performed by the authors of the papers or by a reliable author, three of those algorithms are implemented using software tool "IMAGE ENHANCEMENT PROCESS TOOL" [32]–[33]. The method proposed in this paper can be applied in 30-60m depth and the light source is artificial light. The natural light is not considered at the moment. The underwater images with five different scenes used in experiments have significant blurring of details, color distortion, low brightness, and contrast.

To ensure the fairness of the comparison results, all experimental results were generated on the same computer. The computer was configured as Intel(R) Core(TM) i7-8650U CPU @ 2.11 GHz, 16.00 GB memory, Windows 10 system and x64 processor. MatlabR2017a is software platform.

A. SUBJECTIVE PERFORMANCE EVALUATION

As shown in Fig.7, Fig.7 (a) shows some underwater images of some websites and live-action shots as original images, where (1) (3) (4) comes from web, (2) from the example image in reference [4], and (5) was taken by the underwater robot BlueROV2 in April 2019. Fig.7 (b) shows the results of HE's dark channel prior [4], Fig.7 (c) is the enhanced image obtained by the automatic color enhancement(ACE) of P.G [25], Fig.7 (d) shows the results of Bianco's Lab Color Correction(LAB) [26], Fig.7 (e) is the enhanced image obtained by Screened Poisson equation (SP) [28], Fig.7 (f) is the enhanced image obtained by the gray world algorithm of D.A [23], and Fig.7 (g) shows that the result of Zhu's algorithm, which combined the dark channel prior and histogram equalization [8], and the effect of Fig. 7 (h) obtained by the method proposed in this paper.

As shown in Fig.7, the dark channel prior represented by (b) is not ideal for the underwater image dehazing, and there is still a problem common to the method: the image is too dark. Fig.7 (c) is the effect of the ACE algorithm. It can be seen from the Fig.7 (c) that the ACE algorithm works well in dehazing and color correction, but the brightness is dark. Fig.7 (d) shows the effect of LAB, which has little change from the original image. Fig.7 (e) is the effect of the SP algorithm, it can achieve dehazing, but the color deviation and brightness are not significantly improved. Fig.7 (f) shows that although the gray world can solve the problem of lack of red light in underwater images, it cannot improve the brightness and dehazing, and it over-adjusts the color deviation and distorts the image. Compared with the two methods Fig.7 (b) and Fig.7 (f), Fig. 7(g) has an improvement in brightness, but the effect of color correction on underwater images is not satisfactory. Fig.7 (h) shows the effect of our algorithm, which removes haze, improves brightness and corrects underwater image color deviation, but needs to be improved for local brightness and contrast, and the color correction of Fig.7 (3) and (4) is slightly worse than ACE.

B. QUESTIONNAIRE

For subjective performance evaluation, we designed a questionnaire to evaluate the underwater image enhancement algorithms. A panel of review in the field of underwater imagery (members of the National Key R&D Program of China) was assembled. This panel is composed of several professional fields, such as the field of computer vision, underwater image processing, painting and other professional fields with experience in underwater imagery. This panel

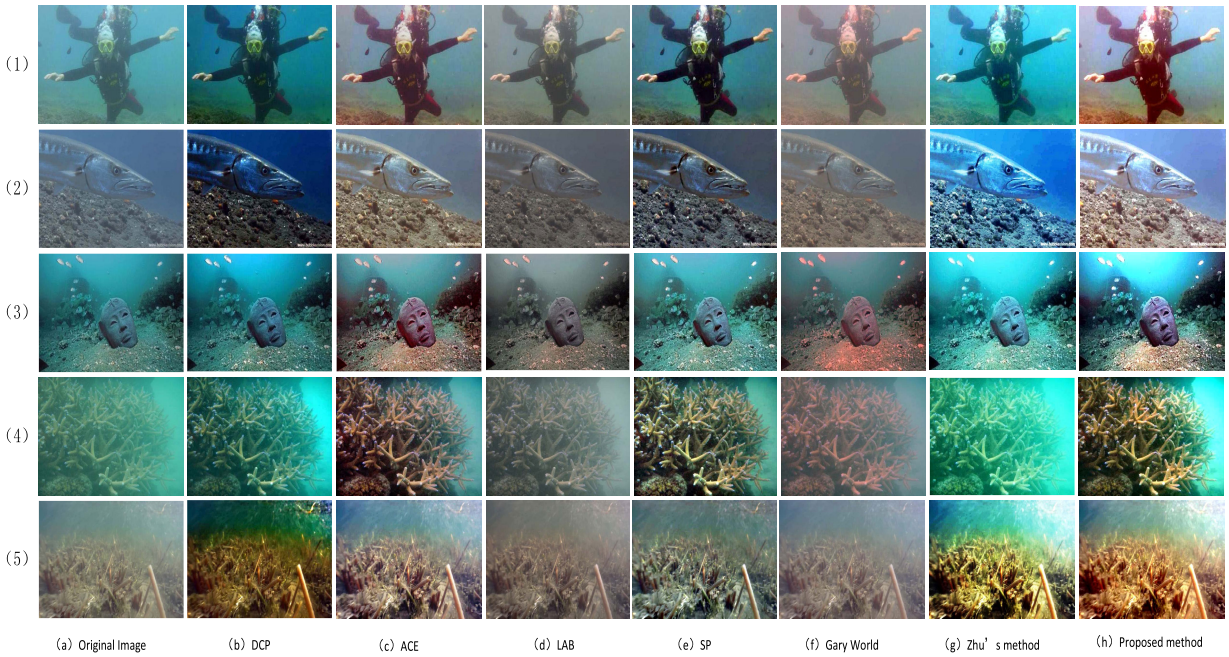

FIGURE 7. Underwater image enhancement. (a) Original image. (b) DCP. (c) ACE. (d) LAB. (e) SP. (f) Gray world. (g) Zhu's method. (h) Proposed method.

TABLE 1. Average value of each algorithm.

	DCP	ACE	LAB	SP	GW	Zhu	Proposed
(1)	6.52	8.06	6.74	7.16	6.76	7.10	**8.18**
(2)	5.94	8.20	6.14	7.24	6.06	7.50	**8.36**
(3)	7.14	**8.30**	6.86	7.50	6.26	6.74	8.14
(4)	7.10	**8.16**	6.22	7.58	5.34	5.48	7.88
(5)	5.60	7.72	6.52	7.46	5.74	6.62	**8.06**
Average	6.46	8.08	6.49	7.34	6.03	6.68	**8.12**

expressed an evaluation of the quality of the enhancement conducted on the underwater images through some selected algorithms [31].

The questionnaire is composed of five underwater images and seven enhancement methods. Each of the enhanced images is labeled with the acronym of the algorithm that produced them. Then, the evaluator was to provide an evaluation expressed as a number from one to ten, where "one" represents a very poor enhancement and "ten" a very good one. The score can only be accurate to two decimal place. All these evaluations, expressed by each evaluator on each enhanced image, provide a lot of data that needs to be interpreted.

Table 1 shows the results of the average value of each algorithm. Except for (3) and (4), the methods proposed in this paper all obtained the highest average value. The ACE algorithm obtained the highest average value on (3) and (4). By analyzing the enhanced image, it can be concluded that the image (3) and (4) processed by the ACE algorithm is superior to our algorithm in color correction, but not all. This is because the method proposed in this paper relies on the accuracy of the maximum scene depth, so the effect of color correction has slight fluctuations. But in general, the total average score of our algorithm is 8.12, which is superior to other enhancement algorithms.

To further analyze the questionnaire and verify the validity of our algorithms, we performed ANOVA (ANalysis Of VAriance) on these data. The purpose is to determine whether the difference between the average score of the algorithms is significant. Also, to determine which algorithms are effectively better than the others, we conducted a "post hoc" analysis, named LSD (Least-significant Difference), which is a test that determines specifically which groups are significantly different [31]. Table 2 shows that there is significances between the seven algorithms.

TABLE 2. ANOVA test results and LSD analysis.

Image	Source	SS	df	MS	F	Sig.
(1)	Between Groups	51.543	6	8.590	28.724	.000
	Within Groups	39.776	133	.299		
	Total	91.319	139			
(2)	Between Groups	126.327	6	21.054	30.227	.000
	Within Groups	92.640	133	.697		
	Total	218.967	139			
(3)	Between Groups	67.127	6	11.188	25.690	.000
	Within Groups	57.920	133	.435		
	Total	125.047	139			
(4)	Between Groups	158.423	6	26.404	48.248	.000
	Within Groups	72.784	133	.547		
	Total	231.207	139			
(5)	Between Groups	110.839	6	18.473	29.933	.000
	Within Groups	82.080	133	.617		
	Total	192.919	139			

A comprehensive analysis of Figure 7, Table 2 and the LSD results (as shown in the appendix) leads to the following conclusions:

Image (1): ACE and our algorithm are significantly better than other algorithms, but ACE and our algorithm do not show significant differences;

Image (2): ACE and our algorithm are better than other algorithms. The effect of SP is not ideal. There is no significant difference between GW, DCP and LAB;

Image (3): ACE and our algorithm are better than other algorithms. The ZHU's algorithm is not significantly different with the LAB. The effect of all algorithms are better than GW;

Image (4): The ACE algorithm is superior to our algorithm and the SP, and these three algorithms are significantly better than the other algorithms;

Image (5): Our algorithm is better than ACE and SP, and the effects of GW and DCP are not ideal.

In a nutshell, our algorithm works well for the processing effect of all underwater images. And our algorithm is not significantly different with the ACE algorithm. So we need another assessment method to verify the superiority of our algorithm.

C. OBJECTIVE PERFORMANCE EVALUATION

Since the underwater image cannot obtain the waterless image as reference, we should select the no-reference quality assessment indicators to evaluate the image. The sharpness is an important indicator to measure image quality, which can better correspond to the subjective feelings of humans [34]. This paper selects several popular and representative no-reference evaluation quality assessment indicators to represent the enhancement image quality. The average gradient [35] can reflect the details contrast and the texture change. Generally, the larger average gradient, the richer the image hierarchy and the clearer the image. No-reference structural sharpness (NRSS) [36] is an improvement based on structural similarity index (SSIM), which uses the characteristics of human vision to be most sensitive to horizontal and vertical edge information, using Sobel operator to extract the edge information of horizontal direction and vertical direction, then calculates the edge information variance. So the larger the value of NRSS, the higher the image quality. The entropy function based on statistical features is also an important indicator to assess the richness of image information. The larger the entropy, the more information, the clearer the image. All three evaluation indicators can well reflect the clarity of the enhancement image and the richness of the details. The evaluation results are shown in Table 3.

According to Table 3, the NRSS values of the enhanced images obtained by our algorithm are all better than the other three algorithms, indicating that the images processed by our algorithm have more detailed information. However, for the average gradient and the entropy function, our algorithm are not the best for Fig.7 (2) and (5), but the method second only to Zhu. This is because the concentrated gray level of the image is "stretched" by the histogram equalization, which makes the picture have higher contrast, so the image has larger gradient. However, regarding to the subjective visual image, excessive stretching of the gray level causes the image to appear undesired information, and the visual experience is not ideal.

TABLE 3. Objective performance evaluation results.

Image	Method	Mean gradient	NRSS	Entropy function
(1)	(a) Original image	1.8251	0.9459	6.0479
	(b) HE's method	2.5587	0.9863	6.6023
	(c) ACE	4.0307	0.9583	7.3244
	(d) LAB	2.0463	0.9434	6.6987
	(e) SP	3.8082	0.9113	7.0052
	(f) Gray world	1.8623	0.9485	6.3891
	(g) Zhu's method	3.3347	0.9687	7.3677
	(h) Our results	**4.4547**	**0.9897**	**7.7151**
(2)	(a) Original image	2.1135	0.9445	5.6419
	(b) DCP	4.6346	0.9434	6.4330
	(c) ACE	5.3819	0.9507	6.9048
	(d) LAB	2.6799	0.9443	5.8779
	(e) SP	5.0799	0.9438	6.5673
	(f) Gray world	2.5259	0.9045	5.7661
	(g) Zhu's method	**7.2590**	0.9098	**7.3799**
	(h) Our results	5.4123	**0.9521**	6.8905
(3)	(a) Original image	6.3660	0.9587	6.9273
	(b) DCP	7.5406	0.9755	7.1153
	(c) ACE	12.0871	0.9783	7.6077
	(d) LAB	7.0261	0.9780	7.1738
	(e) SP	9.9396	0.9837	7.2729
	(f) Gray world	6.8159	0.9658	6.9572
	(g) Zhu's method	10.6933	0.9863	7.5789
	(h) Our results	**12.2360**	**0.9879**	**7.8155**
(4)	(a) Original image	3.0747	0.9492	6.5321
	(b) DCP	5.5386	0.9303	7.2225
	(c) ACE	7.4584	0.9379	7.4342
	(d) LAB	3.4146	0.9517	6.8330
	(e) SP	9.1571	0.9535	7.5124
	(f) Gray world	3.2729	0.9617	6.4552
	(g) Zhu's method	5.6979	0.9269	7.2709
	(h) Our results	**10.0880**	**0.9668**	**7.5674**
(5)	(a) Original image	1.6288	0.9757	6.4673
	(b) DCP	3.2277	0.9745	6.9361
	(c) ACE	3.5267	0.9850	7.3248
	(d) LAB	1.8114	0.9885	6.6414
	(e) SP	3.6306	0.9693	6.8466
	(f) Gray world	1.5596	0.9697	6.4332
	(g) Zhu's method	4.8959	0.9529	**7.9232**
	(h) Our results	**6.4556**	**0.9948**	7.7933

Comprehensive analysis, our algorithm and the ACE algorithm is superior to the other five methods. And our algorithm is similar to the effect of the ACE algorithm, but the scores of three assessment indicators of our algorithm are higher than the ACE algorithm. Except that, after testing a large number of underwater images, our algorithm gets better results more often.

V. CONCLUSION

The adaptive background light estimation proposed in this paper can effectively improve the color deviation caused by red light attenuation and image blur caused by light scattering, and increase the image contrast. Also, the method in this paper extracts data from the image itself, which makes the enhanced image more consistent with the original image and achieves image adaptive enhancement.

However, the accuracy of scene depth estimation has an impact on our method. Since the salinity and the number of suspended particles in the water vary with time, location and season, the accuracy of the scene depth estimation are also relatively reduced. Even accurate depth of the scene cannot be obtained in transitional turbid waters. Therefore, the method

TABLE 4. "Post hoc" analysis results.

Algorithm Name	Algorithm Name	Significance (1)	(2)	(3)	(4)	(5)
DCP	ACE	.000	.000	.000	.000	.000
	LAB	.206	.450	.182	.000	.000
	SP	.000	.000	.087	.042	.000
	Gray World	.168	.650	.000	.000	.574
	Zhu's method	.001	.000	.057	.000	.000
	Our method	.000	.000	.000	.001	.000
ACE	DCP	.000	.000	.000	.000	.000
	LAB	.000	.000	.000	.000	.000
	SP	.000	.000	.000	.014	.297
	Gray World	.000	.000	.000	.000	.000
	Zhu's method	.000	.009	.000	.000	.000
	Our method	.489	.545	.445	.233	.173
LAB	DCP	.206	.450	.182	.000	.000
	ACE	.000	.000	.000	.000	.000
	SP	.016	.000	.003	.000	.000
	Gray World	.908	.762	.005	.000	.002
	Zhu's method	.039	.000	.566	.002	.688
	Our method	.000	.000	.000	.000	.000
SP	DCP	.000	.000	.087	.042	.000
	ACE	.000	.000	.000	.014	.297
	LAB	.016	.000	.003	.000	.000
	Gray World	.022	.000	.000	.000	.000
	Zhu's method	.729	.326	.000	.000	.001
	Our method	.000	.000	.003	.202	.017
Gray World	DCP	.168	.650	.000	.000	.574
	ACE	.000	.000	.000	.000	.000
	LAB	.908	.762	.005	.000	.002
	SP	.022	.000	.000	.000	.000
	Zhu's method	.051	.000	.023	.551	.001
	Our method	.000	.000	.000	.000	.000
Zhu's method	DCP	.001	.000	.057	.000	.000
	ACE	.000	.009	.000	.000	.000
	LAB	.039	.000	.566	.002	.688
	SP	.729	.326	.000	.000	.001
	Gray World	.051	.000	.023	.551	.001
	Our method	.000	.001	.000	.000	.000
Our method	DCP	.000	.000	.000	.001	.000
	ACE	.489	.545	.445	.233	.173
	LAB	.000	.000	.000	.000	.000
	SP	.000	.000	.003	.202	.017
	Gray World	.000	.000	.000	.000	.000
	Zhu's method	.000	.001	.000	.000	.000

in this paper dose not apply to ultra-turbid waters with low visibility. The above problem may be solved by combining with sonar imaging. Besides, the dark channel of the object in the clear image mostly tends to zero, that is, the dark channel value is zero when the maximum scene depth is on the object. In this case, the background light A (λ) should take the value of the maximum scene depth of the original image. In addition to the above two cases, the adaptive background light estimation method proposed in this paper is satisfactory for underwater image enhancement and provides a new method for underwater image enhancement.

APPENDIX

See Table. 4.

REFERENCES

[1] R. A. Armstrong, O. Pizarro, and C. Roman, "Underwater robotic technology for imaging mesophotic coral ecosystems," in *Mesophotic Coral Ecosystems* (Coral Reefs of the World), vol. 12. Cham, Switzerland: Springer, 2019, pp. 973–988.

[2] R. Wang, Y. Wang, J. Zhang, and X. Fu, "Review on underwater image restoration and enhancement algorithms," in *Proc. 7th Int. Conf. Internet Multimedia Comput. Service (ICIMCS)*, 2015, pp. 56–62.

[3] H. Lu, Y. Li, Y. Zhang, M. Chen, S. Serikawa, and H. Kim, "Underwater optical image processing: A comprehensive review," *Mobile Netw. Appl.*, vol. 22, no. 6, pp. 1204–1211, 2017.

[4] K. He, J. Sun, and X. Tang, "Single image haze removal using dark channel prior," *IEEE Trans. Pattern Anal. Mach. Intell.*, vol. 33, no. 12, pp. 2341–2353, Dec. 2011.

[5] H. Y. Yang, P. Y. Chen, and C. C. Huang, "Low complexity underwater image enhancement based on dark channel prior," in *Proc. 2nd Int. Conf. Innov. Bio-Inspired Comput. Appl.*, Dec. 2011, pp. 17–20.

[6] A. Galdran, D. Pardo, A. Picón, and A. Alvarez-Gila, "Automatic red-channel underwater image restoration," *J. Vis. Commun. Image Represent.*, vol. 26, pp. 132–145, Jan. 2015.
[7] X. Ding, Y. Wang, J. Zhang, and X. Fu, "Underwater image dehaze using scene depth estimation with adaptive color correction," in *Proc. OCEANS*, Aberdeen, U.K., Jun. 2017, pp. 1–5.
[8] W. Q. Zhu, J. Yu, and S. Y. Xi, "Underwater image restore based on dark channel prior and contrast enhancement," *Inf. Technol.*, vol. 8, no. 13, pp. 54–57, Aug. 2017.
[9] C. O. Ancuti, C. Ancuti, C. De Vleeschouwer, and P. Bekaert, "Color balance and fusion for underwater image enhancement," *IEEE Trans. Image Process.*, vol. 27, no. 1, pp. 379–393, Jan. 2018.
[10] H. L. Xie, G. H. Peng, and F. Wang, "Underwater image restoration based on background light estimation and dark channel prior," *Acta Opt. Sinica*, vol. 38, no. 1, pp. 18–27, 2018.
[11] Y. J. Li, J. R. Li, Y. Li, and H. Kim, "Low-light underwater image enhancement for deep-sea tripod," *IEEE Access*, vol. 7, pp. 44080–44086, Apr. 2019.
[12] D. Akkaynak and T. Treibitz, "Sea-thru: A method for removing water from underwater images," in *Proc. IEEE Conf. Comput. Vis. Pattern Recognit.*, Jun. 2019, pp. 1682–1691.
[13] B. L. McGlamery, "A computer model for underwater camera systems," *Proc. SPIE*, vol. 208, pp. 221–231, Mar. 1980.
[14] J. Y. Chiang and Y.-C. Chen, "Underwater image enhancement by wavelength compensation and dehazing," *IEEE Trans. Image Process.*, vol. 21, no. 4, pp. 1756–1769, Apr. 2012.
[15] L. A. Torres-Méndez and G. Dudek, "Color correction of underwater images for aquatic robot inspection," in *Proc. EMMCVPR*, in Lecture Notes in Computer Science, vol. 3757, 2005, pp. 60–73.
[16] I. Laina, C. Rupprecht, V. Belagiannis, F. Tombari, and N. Navab, "Deeper depth prediction with fully convolutional residual networks," in *Proc. IEEE Int. Conf. 3D Vis. (3DV)*, Oct. 2016, pp. 239–248.
[17] A. B. Owen, "A robust hybrid of lasso and ridge regression," *Contemp. Math.*, vol. 443, no. 7, pp. 59–72, 2007.
[18] L. Zwald and S. L. Lacroix, "The berhu penalty and the grouped effect," Jul. 2012, *arXiv:1207.6868*. [Online]. Available: https://arxiv.org/abs/1207.6868
[19] K. He, X. Zhang, S. Ren, and J. Sun, "Deep residual learning for image recognition," 2015, *arXiv:1512.03385*. [Online]. Available: https://arxiv.org/abs/1512.03385
[20] P. K. Nathan Silberman, D. Hoiem, and R. Fergus, "Indoor segmentation and support inference from RGBD images," in *Proc. ECCV*, 2012, pp. 746–760.
[21] A. Saxena, M. Sun, and A. Y. Ng, "Make3D: Learning 3D scene structure from a single still image," *IEEE Trans. Pattern Anal. Mach. Intell.*, vol. 31, no. 5, pp. 824–840, May 2009.
[22] Q. Zhu, J. Mai, and L. Shao, "A fast single image haze removal algorithm using color attenuation prior," *IEEE Trans. Image Process.*, vol. 24, no. 11, pp. 3522–3533, Nov. 2015.
[23] K. Zuiderveld, "Contrast limited adaptive histogram equalization," in *Graphics Gems IV*, P. Heckbert, Ed. New York, NY, USA: Academic, 1994.
[24] D. A. Forsyth, "A novel algorithm for color constancy," *Int. J. Comput. Vis.*, vol. 5, no. 1, pp. 5–35, 1990.
[25] P. Getreuer, "Automatic color enhancement (ACE) and its fast implementation," *Imag. Process. Line*, vol. 2, pp. 266–277, Nov. 2012.
[26] G. Bianco, M. Muzzupappa, F. Bruno, R. Garcia, and L. Neumann, "A new color correction method for underwater imaging," *Int. Arch. Photogramm., Remote Sens. Spatial Inf. Sci.*, vol. 40, no. 5, pp. 25–32, 2015.
[27] D. Berman and S. Avidan, "Non-local image dehazing," in *Proc. IEEE Conf. Comput. Vis. Pattern Recognit.*, Jun. 2016, pp. 1674–1682.
[28] J.-M. Morel, A.-B. Petro, and C. Sbert., "Screened Poisson equation for image contrast enhancement," *Image Process. On Line*, vol. 4, pp. 16–29, Mar. 2014.
[29] S. Suwajanakorn and C. Hernandez, "Depth from focus with your mobile phone," in *Proc. IEEE Conf. Comput. Vis. Pattern Recognit.*, Jun. 2015, pp. 3497–3506.
[30] P. Drews-Jr, E. R. Nascimento, S. S. C. Botelho, and M. F. M. Campos, "Underwater depth estimation and image restoration based on single images," *IEEE Comput. Graph. Appl.*, vol. 36, no. 2, pp. 24–35, Mar./Apr. 2016.
[31] W. Zhu, R. Hu, and L. G. Liu, "Grey conversion via perceived-contrast," *Vis. Comput.*, vol. 30, no. 3, pp. 299–309, 2014.
[32] M. Mangeruga, F. Bruno, M. Cozza, P. Agrafiotis, and D. Skarlatos, "Guidelines for underwater image enhancement based on benchmarking of different methods," *Remote Sens.*, vol. 10, no. 10, pp. 1652–1679, 2018.
[33] M. Mangeruga, M. Cozza, and F. Bruno, "Evaluation of underwater image enhancement algorithms under different environmental conditions," *J. Mar. Sci. Eng.*, vol. 6, no. 1, pp. 10–23, 2018.
[34] A. K. Moorthy and A. C. Bovik, "Blind image quality assessment: From natural scene statistics to perceptual quality," *IEEE Trans. Image Process.*, vol. 20, no. 12, pp. 3350–3364, Dec. 2011.
[35] J.-B. Wang, N. He, L.-L. Zhang, and K. Lu, "Single image dehazing with a physical model and dark channel prior," *Neuro Comput.*, vol. 149, pp. 718–728, Feb. 2015.
[36] X. Xie, J. Zhou, and Q. Wu, "No-reference quality index for image blur," *J. Comput. Appl.*, vol. 30, no. 4, pp. 921–924, 2010.

SHUDI YANG received the B.S. degree in mechanical engineering and the M.S. degree in safety engineering from the North China Institute of Science and Technology, in 2014 and 2017, respectively. She is currently pursuing the Ph.D. degree in vehicle engineering with the University of Science and Technology Beijing. Her research interests include computer vision, image processing, and deep learning.

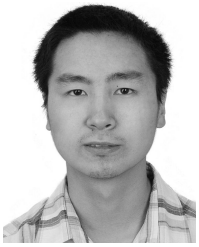

ZHEHAN CHEN received the Ph.D. degree in industrial engineering from the Beijing University of Aeronautics and Astronautics, Beijing, China, in 2013. He is currently an Associate Professor with the School of Mechanical Engineering, University of Science and Technology Beijing. His research interests mainly focus on the technologies of intelligent manufacturing in the industrial 4.0 era, which include human–machine collaboration based on AI, industrial data mining and applications, and implementations of industrial information systems.

ZHIPENG FENG received the Ph.D. degree in power machinery and engineering from the Dalian University of Technology, Dalian, China, in 2003. He is currently a Professor with the School of Mechanical Engineering, University of Science and Technology Beijing. His research interests mainly focus on machinery fault diagnosis, signal processing, artificial intelligence, and mechanical dynamics.

XIAOMING MA received the bachelor's degree in mechanical and electrical engineering from the School of Mechanical Engineering, Yanshan University. He is currently pursuing the master's degree with the School of Mechanical Engineering, University of Science and Technology Beijing. His research interests mainly focus on computer vision and image processing.